THE ASTROPHYSICAL JOURNAL, 208:662–672, 1976 September 15

MOTIONS OF THE STARS AND THE EXCITED GAS IN THE BARRED SPIRAL GALAXY NGC 3351

CHARLES J. PETERSON, VERA C. RUBIN,† W. KENT FORD, JR.,† AND NORBERT THONNARD
Department of Terrestrial Magnetism, Carnegie Institution of Washington
Received 1976 January 30

ABSTRACT

The velocity field of the spiral-arm region of the bright barred spiral NGC 3351 has been determined from measurements of emission lines on spectra from the 4 meter Mayall telescope. The *stellar* velocity field of the bar also has been obtained by measurement of relatively sharp absorption features; the sharpness of the absorption lines is due to the small velocity dispersion along the line of sight, $\sigma = 140 \pm 30$ km s^{-1}. The bar is rotating with a constant angular velocity of 80 ± 20 km s^{-1} kpc^{-1} and therefore is a quasi-stationary feature of the galaxy. There is no evidence for excited gas in the bar. Beyond the region of the bar, the velocities of the H II regions in the spiral arms are consistent with a pattern of circular motion only, with the rotation curve reaching a maximum of $V_{rot} \approx 220$ km s^{-1} at $R \approx 3$–5 kpc and decreasing to $V_{rot} \approx 170$ km s^{-1} at $R \approx 8$ kpc. Noncircular motions have, however, been observed in the nuclear regions of NGC 3351. The kinematical major axis is the same as the line of nodes determined from the apparent ellipse formed by the projection of the galaxy on the plane of the sky. The systematic velocity of the galaxy is 779 ± 3 km s^{-1}, both from optical and from 21 cm neutral hydrogen data.

Subject headings: galaxies: individual — galaxies: internal motions — stars: stellar dynamics

I. INTRODUCTION

NGC 3351 (M95: $\alpha_{1950} = 10^{h}41^{m}.3$, $\delta_{1950} = +11°58'$) is one of the few bright barred spiral [SBb or SB(r)b] galaxies in the northern sky. It is a particularly good candidate in which to search for noncircular motions of the stellar population in the bar because the galaxy is oriented on the sky with the bar only a few degrees from the minor axis. In addition, the advent of the Mayall 4 m telescope coupled with a fast image-tube spectrograph has only recently made possible the acquisition of well-exposed spectra along the bar and spectra with measurable emission lines from the faint emission regions in the spirals arms. A previous study (Rubin, Ford, and Peterson 1975, hereafter called Paper I) was limited to the velocity field of excited gas near the nucleus. Information on the velocity field of the bar and the outer regions is fundamental in attempting to model the dynamics of barred systems.

In this paper we study the velocity pattern of the bar and the outer ring of the spiral arm region.

† Visiting Astronomer, Kitt Peak National Observatory, which is operated by the Association of Universities for Research in Astronomy, Inc., under contract with the National Science Foundation.

II. OBSERVATIONS

NGC 3351 shows a bright nucleus, a broad bar, and two spiral arms which originate at the ends of the bar and circle the galaxy to form an almost perfect outer ring with a radius of ~60″. At the adopted distance of

TABLE 1

RECORD OF 4 METER SPECTROSCOPIC OBSERVATIONS

Position number	Plate		Date	Dispersion (Å/mm)	Exposure (min.)	Position angle (degrees)		Lines measured
1	4M-109	a	1974 Mar 17	54	30	90°	through nucleus	Hα, [NII], [SII]
		b			60	90	through nucleus	Hα, [NII], [SII]
2	4M-113		1974 Mar 18	54	120	90*	north of nucleus	Hα, [NII]
3	4M-584	a	1975 Jan 16	53	120	62.1*	northwest	Hα, [NII], [SII]
4		b			120	137.8*	northeast	Hα, [NII], [SII]
5	4M-589	a	1975 Jan 17	53	90	50.9*	southeast	Hα, [NII]
6		b		53	90	26.0*	east	Hα, [NII]
7	4M-591		1975 Jan 17	53	90	88.1*	south	Hα, [NII]
8	4M-593	b	1975 Jan 18	53	90	164.3*	west	Hα, [NII]
9	4M-594	a	1975 Jan 18	53	90	19.0*	west	Hα, [NII]
10		b		53	45	23.0*	east	Hα, [NII]
11	4M-596		1975 Jan 19	53	140	117.0	along bar	Hβ, Hγ, absorption lines
12	4M-807		1975 May 4	49	168	112.0	along bar	Hβ, Hγ, Hδ, absorption lines

* Slit aligned along outer ring

TABLE 2A

Emission-Line Velocities (Heliocentric)

Line	x* arc sec	y* arc sec	v km s^{-1}
Plate 4m-109a PA 90°			
[NII]λ 6548	0.0	0.0	764
	9.3		799
	-79.3		754
	-4.8		681
	0.0		757
	3.3		796
	4.7		793
	6.6		804
	9.2		828
	10.3		847
[NII]λ 6583	-22.1		725
	-16.9		734
	-11.3		752
	-4.0		734
	0.0		761
	5.0		793
	9.9		810
[SII]λ 6717	0.0		770
	4.8		835
	9.6		837
[SII]λ 6731	0.0		774
	4.3		857
	9.2		849
Plate 4m-109b PA 90°			
[NII]λ 6548	0.0	0.0	788
	9.4		837
Hα	-79.2		761
	-3.8		700
	-1.7		750
	0.0		758
	2.2		815
	4.5		848
	10.0		842
[NII]λ 6583	0.0		758
	4.6		814
	9.3		816
[SII]λ 6717	0.0		791
	4.3		834
	9.5		851
[SII]λ 6731	0.0		791
	4.5		808
	9.1		887
Plate 4m-113 PA 90°			
Hα	-85.9	-173.0	647
	-77.8		647
	-70.7		647
	-20.0		651
	14.8		643
	2.6		645
	25.0		659
	43.6		710
[NII]λ 6583	-20.1		670
	2.8		639
	25.0		640
Plate 4m-589a PA 50°9			
Hα	-134.4	26.8	694
	-87.2	-11.5	744
	-57.1	-35.9	834
	-51.2	-40.8	825
	-43.9	-46.7	854
	-38.4	-51.2	880
	-35.5	-53.5	876
	-33.5	-55.1	856
	-29.0	-58.8	892
	-24.2	-62.7	895
	-21.7	-64.8	890
	-19.2	-66.8	923
	-16.2	-69.2	911
	-13.8	-71.1	915
	- 6.5	-77.1	923
	- 2.9	-80.0	936
	-0.3	-82.5	928
	3.7	-85.4	918
	6.2	-87.4	924
	8.4	-89.2	924
	16.9	-96.1	890
	28.5	-105.5	924
	83.3	-150.0	858
[NII]λ 6583	-51.8	-40.3	832
	-38.8	-50.8	923
	-29.0	-58.8	908
	-13.7	-71.3	953
	2.2	-84.1	942
	82.8	-149.7	881
Plate 4m-584b PA 137°8			
Hα	-85.0	0.7	763
	-46.7	43.6	661
	-42.0	48.8	659
	-39.3	51.7	645
	-32.8	58.9	649
	-22.4	70.4	648
	-20.0	73.0	638
	-17.8	75.4	637
	-13.3	80.4	631
	-10.3	83.7	620
	22.1	119.4	664
	24.3	121.8	649
[NII]λ 6583	-85.0	0.6	781
	-40.6	50.3	654
	-20.0	73.0	642
	-10.9	83.0	635
	23.4	120.9	654
[SII]λ 6717	-85.8	0.4	769
	-20.0	73.0	651
[SII]λ 6731	-85.4	0.8	744
	-20.1	72.9	635
Plate 4m-584a PA 62°1			
[NII]λ 6548	2.1	73.0	678
	-80.5	116.7	661
	-18.8	84.0	631
	-16.0	82.5	624
	-5.7	77.1	663
	2.0	73.0	647
	17.8	64.6	655
	25.0	60.8	672
	37.4	54.2	677
	92.5	25.1	770
	96.9	22.7	761
	118.4	11.4	785
[NII]λ 6583	-17.2	83.2	629
	2.0	73.0	654
	17.7	64.7	657
	118.4	11.4	800
[SII]λ 6717	1.9	73.0	658
	17.9	64.6	690
[SII]λ 6731	2.0	73.0	661
Plate 4m-589b PA 26°			
Hα	-137.0	128.3	687
	-130.5	114.9	675
	-118.5	90.3	686
	-80.9	13.2	756
	-78.0	7.4	783
	-76.9	-5.1	788
	-72.0	-5.0	814
	-69.4	-10.3	793
	-48.5	-53.3	879
	-36.6	-77.6	876
[NII]λ 6583	-80.8	12.9	747
	-72.1	-4.8	855
Plate 4m-591 PA 88°1			
Hα	-40.2	-49.7	849
	-36.8	-49.8	866
	-33.3	-49.9	847
	6.6	-51.2	904
	16.0	-51.5	897
	19.2	-51.6	896
	29.1	-52.0	897
	34.1	-52.1	926
	37.3	-52.2	903
	40.9	-52.4	879
	44.2	-52.5	898
	48.5	-52.6	921
	111.8	-54.7	862
[NII]λ 6583	-37.6	-49.7	939
	19.3	-51.6	916
Plate 594b PA 23°0			
Hα	31.6	67.0	654
	33.7	61.9	634
	35.1	58.6	672
	37.4	53.2	657
	55.9	9.7	769
	60.0	0.0	818
	61.3	-2.9	761
	62.6	-6.2	833
[NII]λ 6583	35.0	58.9	727
	60.2	-0.4	831
	62.3	-5.4	834
Plate 4m-593b PA 164°3			
Hα	29.1	-109.5	879
	29.9	-106.9	843
	46.2	-49.0	901
	47.0	-45.9	879
	47.8	-43.1	896
	49.0	-38.9	913
	52.1	-27.8	862
	53.7	-22.2	866
	54.5	-19.2	845
	55.6	-15.3	815
	57.0	-10.3	853
	61.3	4.9	778
	62.9	10.6	772
	70.7	38.1	752
	71.2	40.1	761
[NII]λ 6583	47.1	-45.7	912
	54.3	-20.1	860
	57.0	-10.3	852
	63.0	10.8	779
	70.9	39.1	771
Plate 4m-594a PA 19°0			
Hα	-98.0	130.0	628
	-87.0	98.3	635
	-77.7	71.1	623
	-72.6	56.2	675
	-69.7	47.8	651
	-64.6	33.2	674
	-60.6	21.4	690
	-58.3	14.9	703
	-56.9	10.6	709
	-53.5	1.0	702
	-51.8	-4.2	704
	-50.2	-8.9	710
	-42.1	-32.3	747
	-40.4	-37.1	763
	-38.9	-41.7	823
	-36.0	-50.0	811
	-35.1	-52.6	798
	-29.9	-67.7	822
	-24.4	-83.8	871
	-21.0	-93.6	891
	-19.9	-96.7	897
	-11.8	-120.3	839
[NII]λ 6583	-58.4	15.1	685
	-57.0	10.9	693
	-40.5	-37.0	813
	-36.0	-50.0	837
	-19.6	-97.6	944
	-12.0	-119.7	876
Plate 4m-596 PA 117°			
Hγ	-54.3	-27.6	834
	86.8	44.3	744
	89.1	45.4	779
	90.7	46.2	746
Hβ	-63.8	-32.5	868
	-60.5	-30.8	866
	-56.8	-28.9	857
	-53.5	-27.3	840
	-48.2	-24.6	842
	-42.7	-21.7	844
	50.5	25.7	759
	54.8	27.9	748
	63.2	32.2	735
	75.4	38.4	785
	80.2	40.9	735
	83.0	42.3	758
	86.6	44.1	782
	89.0	45.4	773
	91.4	46.6	767
	103.6	52.8	757
Plate 4m-807 PA 112°			
Hδ	50.2	20.3	768
	58.1	23.5	786
	59.1	23.9	782
	59.8	24.2	806
	91.7	37.0	764
	93.1	37.6	753
	94.4	38.1	743
Hγ	48.8	19.7	752
	50.3	20.3	738
	52.1	21.1	767
	57.8	23.3	722
	59.2	23.9	737
	60.5	24.4	780
	92.6	37.4	740
	93.6	37.8	743
	94.8	38.3	754
Hβ	-148.6	-60.0	825
	49.4	20.0	721
	50.7	20.5	758
	52.5	21.2	801
	57.5	23.2	696
	60.0	24.2	743
	62.0	25.1	760
	91.4	36.9	703
	93.4	37.7	749
	95.2	38.5	768

*x and y form a Cartesian coordinate system, on the plane of the sky, centered on the nucleus, with x positive in the west direction, y positive to the north.

10 Mpc (Paper I), this corresponds to 3 kpc. The mean surface brightness of this ring is ~22 blue magnitudes per square second of arc (Vorontsov-Vel'yaminov and Savel'eva 1974). In order to study the velocity field of the excited gas in this outer region, a series of spectra (Table 1) were obtained in the Hα region with the 4 m Mayall telescope Cassegrain spectrograph and a two-stage Carnegie image tube. The slit was aligned tangential to the outer ring so as to cross bright emission patches in the spiral arms. The orientations of the slit positions are illustrated in Figure 1 (Plate 8). All plates were measured on the Mann two-coordinate measuring engine at the Department of Terrestrial Magnetism. Heliocentric velocities determined from Hα, [N II], and [S II] emission lines are tabulated in Table 2A. A preliminary discussion of the velocity system of the 4 m spectrograph is given in the Appendix.

Because it is of equal importance in understanding the dynamics of barred spiral systems to directly measure the velocity field of the stellar population, two plates were taken in the blue spectral region. On long-exposure spectra along the bar (P.A. 112°, Fig. 2 [Pl. 9]) and slightly offset (P.A. 117°) to the axis of the bar, the positions of relatively sharp absorption lines (H and K of Ca II, Ca I λ4226, Fe I λ4325, and others) were measurable. Mean internal errors for one measurement range from ~20 km s^{-1} for the sharp Ca I λ4226 feature to ~45 km s^{-1} for the intrinsically broader H and K lines of Ca II, compared with errors of ~10–20 km s^{-1} for the hydrogen emission lines on the same spectra.

The absorption line velocities are listed in Tables 2B and 2C and the measures of the absorption line velocities of plate 4M-807 (P.A. 112°, along the bar) are plotted in Figure 3*a*. Figure 3*b* shows the emission line velocities measured from the same spectrum, and Figure 3*c* shows the emission line velocities measured from plate 4M-596 (P.A. 117°). It should be emphasized that the lack of emission line velocities over the angular extent of the bar is not due to overexposure of the spectrum, but rather is due to the lack of detectable emission in this part of the galaxy.

A number of difficulties are involved in the measurement of absorption line velocities. There is the problem of adopting a rest wavelength for the computation of the Doppler velocity. Absorption features may not be symmetrical because of blending of several lines and because of integration along the line of sight through the galaxy. Contamination by night-sky features is not a serious problem in NGC 3351 as its radial velocity shifts features by ~10 Å with respect to the night-sky spectrum. The displacement between the night-sky and galaxy lines is especially noticeable for the strong absorption lines, as for example H and K. Absorption line features were identified by comparison of the galaxy spectra with stellar spectra of the *Bonner Atlas für Objektive Prismen Spektren* (Seitter 1970), and rest wavelengths were initially taken from *A Multiplet Table of Astrophysical Interest* (Moore 1959). In all but one case (the Cr I λ4666 feature which is a blend of several lines), the absorption features could be ascribed principally to absorption by a single atomic species. Comparison of the mean velocity for the galaxy determined from the velocity curve of each absorption line with the adopted systemic velocity of the galaxy (see below) suggested that, due to blending effects, the effective wavelengths of some features needed to be adjusted by as much as 1.5 Å. The adopted rest wavelengths for the measured absorption features are given in Table 3.

Finally, because of the low signal-to-noise ratio, measurements of the apparent centers of the weak, relatively broad absorption lines tend to have a larger scatter than is found for the velocities determined from emission lines of the same plate. To minimize any

TABLE 2B

ABSORPTION LINE VELOCITIES (heliocentric) FROM SPECTRUM 4M-596 P.A. 117°

Radial position (arc sec)	CaI λ4226	FeI λ4325	Hγ λ4340	Cr I λ4666	Radial position (arc sec)	FeI λ4891	Radial position (arc sec)	FeI λ5041	Radial position (arc sec)	MgI λ5183
-54.2 SE	841	770	773	816	-30.2 SE	747	-56.8 SE	805	-54.2 SE	840
-46.2	837	762	796	827	-22.2	755	-48.8	806	-46.2	789
-38.2	833	802	823	828	-14.3 SE	779	-40.9	820	-38.2	777
-30.2	794	765	825	787	+21.7 NW	739	-32.9	826	-30.2	851
-22.2	808	767	770	780	29.6	782	-24.9	833	-22.2	842
-14.3	770	798	845	808	37.6	770	-16.8	797	-14.3 SE	830
-6.3 SE	730	736	840		45.6	786	-8.9 SE	814	9.7 NW	733
+1.7 NW	719				53.6	767	+15.0 NW	742	17.7	771
9.7	775	776	768		61.5	838	23.0	757	25.6	795
17.7	763	756	713	780	69.5	800	31.0	757	33.6	795
25.6	721	803	796	760	77.5 NW	795	38.9	768	41.6	816
33.6	684	815	773	731			46.9	708	49.5	743
41.6	694	818	768	771			54.9	715	57.6	737
49.5	751	808		781			62.9	702	65.5	752
57.6	799						70.9 NW	741	73.5	743
64.2	793								81.5 NW	711
72.2	747									
80.2	757									
88.1 NW	728									

TABLE 2C

Absorption Line Velocities (heliocentric) from Spectrum 4M-807, P.A. = 112°

Radial position (arc sec)	Ca II K λ 3933	Ca II H λ 3968	Fe I λ 4045	Ca I λ 4226	Fe I λ 4325	Hγ λ 4340	Fe I λ 4383	Cr I* λ 4666	Hβ λ 4861
-80.3 SE			796						
-77.6			794						
-75.0			795	837			834		
-72.3			798	817			831		
-69.6			788	810			840		
-67.0			786	813			819		
-64.3			826	816			799		
-61.7			847	817		804	781		
-59.0			769	817		784	787		
-56.3			767	828		795	819		
-53.7			808	751		806	825		
-51.0			820	753	773	826	803	818	
-48.4			789	770	782	822	832	823	
-45.7			752	788	787	836	798	792	
-43.1			756	790	817	832	784	772	
-40.4			757	790	797	825	758	779	
-37.7			776	817	825	817	731	836	765
-35.1			774	822	820	824	755	796	778
-32.4			822	812	800	830	751	762	717
-29.7			823	802	781	833	787	794	810
-27.1			835	769	754	825	737	839	796
-24.4	773		800	792	751	815	763	809	772
-21.7	781		774	778	786	824	794	799	765
-19.1	791		779	770	791	812	787	801	760
-16.5	790		763	780	790	812	778	801	740
-13.8	813		764	785	783	799	741	764	
-11.1	796	815	789	795	802				
-8.4 SE	776	773							
+7.4 NW	763	777		807					
10.0	787	763	769	810					
12.6	785	774	797	794	783	706	753		
15.4	787	768	768	783	799	693	793		
18.1	765	767	788	801	747	715	786		784
20.7	776	804	782	780	765	732	737	776	782
23.4	779	776	800	787	757	718	800	749	778
26.0	756	781	822	773	744	768	801	779	784
28.7	762	739	806	787	753	754	775	760	786
31.3	737	744	790	748	756	762	773	766	772
34.0	740	757	752	748	786	798	748	775	786
36.6		754	752	735	807	772	745	770	784
39.3			779	725	795	758	750	792	810
42.0			784	749	784	756	767	772	783
44.7			769	762	784	737	753	748	
47.3			778	760	789	740	768	752	
50.0			749	777	794		765	756	
52.6			763	796	752		746	734	
55.3			761	847	746		737		
57.9			762	804	751		755		
60.6			733	748	739		774		
63.2			747	710	707		801		
65.9				677			784		
68.6				703			768		
71.3				702			752		
73.9				724					
76.6 NW				720					

* Blend of two lines.

1976ApJ...208..662P

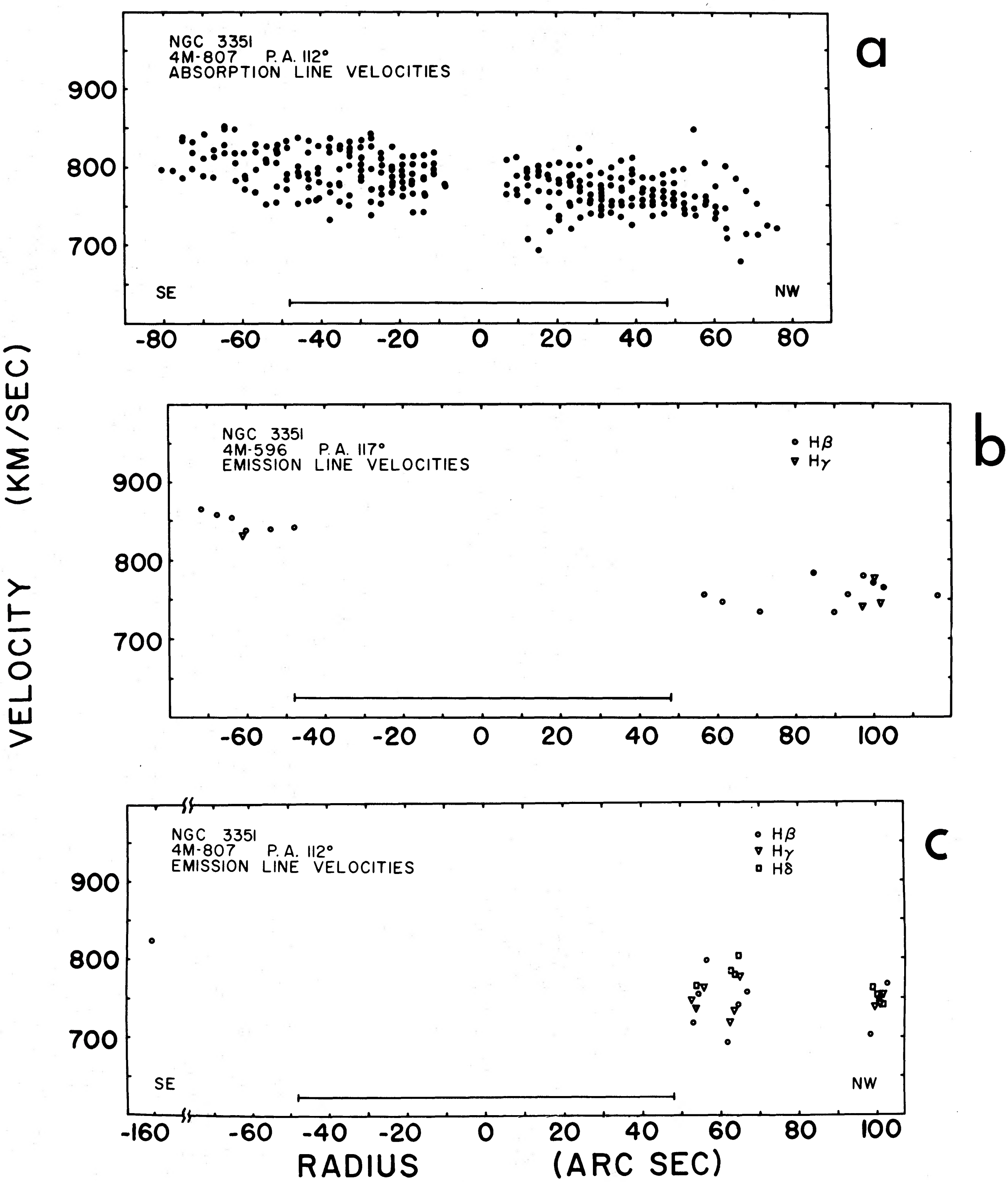

FIG. 3.—(*a*) Observed line-of-sight velocities for stellar absorption lines seen along the position angle (112°) of the bar. The radial extent of the bar is indicated. (*b*) Observed line-of-sight velocities for emission regions seen in the position angle (112°) of the bar. (*c*) Observed line-of-sight velocities for emission regions along position angle 117°.

TABLE 3

EFFECTIVE WAVELENGTHS OF MEASURED ABSORPTION FEATURES

	PLATE 4m-807 PA 112°				PLATE 4m-596 PA 119°		
Identification	λ	ΔV(km/sec)	Δλ	$\lambda_{adopted}$	ΔV(km/sec)	Δλ	$\lambda_{adopted}$
Ca II K	3933.664	-20	-0.25	3933.41			
Ca II H	3968.470	10	0.10	3968.60			
Fe I	4045.815	-20	-0.27	4045.55			
Ca I	4226.728	10	0.14	4226.87	-30	-0.42	4226.31
Fe I	4325.765	6	0.09	4325.85	0	0.00	4325.77
H γ	4340.468	60	0.86	4341.33	-35	-0.52	4339.95
Fe I	4383.547	-10	-0.15	4383.39			
Cr I*	4666.	-55	-0.89	4665.21	-75	-1.18	4664.82
H β	4861.332	100	1.62	4862.95			
Fe I	4891.496				70	1.14	4892.64
Fe I	5041.759				80	1.14	5042.90
Mg I	5183.614				15	0.27	5183.88

* Blend.

systematic errors in the analysis of the absorption line velocity data, all measurements from a number of lines have been plotted together in Figure 3*a*.

III. ANALYSIS OF THE VELOCITY FIELD

The observed velocity field of the galaxy is consistent with a galaxy with only circular motions of the stars and the excited gas. In Figure 4 are plotted hydrogen emission line velocities as a function of angular position in the plane of the galaxy (measured from the northeast major axis). For pure rotation, the data should describe a sinusoidal curve with minimum line-of-sight velocity along the major axis of the approaching side and maximum velocity along the major axis of the receding side. Various subgroups of the data have been used to compute the systemic velocity V_c, the amplitude $V_a = V_{rot}(r) \sin i$, and the position angle of the kinematical major axis θ_0 relative to the adopted major axis in a least-squares solution of the form

$$V = V_c + V_a \cos(\theta + \theta_\theta) .$$

For the initial solution (Table 4), the position angle on the plane of the sky of the northeast major axis, from which all angular positions were measured, was taken to be 18°. This value was adopted in Paper I from a consideration of the orientation of the apparent ellipse formed by the projection of the galaxy on the sky. The initial solution suggested that the line of nodes be adjusted to 15° on the plane of the sky. All successive solutions were made with $\theta_0 = 0°$; angular positions are measured from this adopted northeast major axis position.

The 124 data points give a systemic velocity for NGC 3351 of 779 ± 3 km s^{-1}, in excellent agreement with the central velocity of 779 ± 8 km s^{-1} determined for the contracting ring in the nucleus (Paper I) and 779 ± 3 km s^{-1} from the velocity midpoint of the 21 cm hydrogen line profile obtained with the 91.4 m (300 foot) NRAO telescope[1] (Fig. 5). Table 4 shows that use of various subgroupings of the data does not significantly change this adopted value.

The velocity amplitude of the sinusoidal curve for all the data is $V_a = 139 \pm 4$ km s^{-1} and is in good agreement with the half-width (at a level of 20% of the peak value) of 142 ± 2 km s^{-1} for the 21 cm neutral hydrogen profile. This velocity amplitude corresponds to a circular velocity in the plane of the galaxy of $V_{rot} = 216 \pm 6$ km s^{-1} for an adopted inclination angle of 40° (Paper I). Division of the data into two groups on the basis of radial position (Group I, $60'' < r < 90''$; Group II, $r > 90''$, measured in the plane of the galaxy) suggests that the turnover point in the rotation curve is passed. For the $60'' < r < 90''$ group, $V_a = 143 \pm 5$ km s^{-1}, $V_{rot} = 222 \pm 8$ km s^{-1}; and for the $r > 90''$ group, $V_a = 130 \pm 6$ km s^{-1}, $V_{rot} = 202 \pm 9$ km s^{-1}.

The rotation curve is shown in Figure 6, where all data within 20° (*open circles*) and between 20° and 40° from the major axis (*closed circles*) have been used. The velocity data here also indicate that the turnover point of the rotation curve has been passed.

The lack of excited gas interior to $r = 50''$ (except for the nuclear ring) precludes delineation of this part of the rotation curve by the use of emission lines. The interior part of the rotation curve, $r < 60''$, is obtained from the measurements of the stellar absorption lines. The data of the two spectra are consistent with the inner region of the galaxy being in a state of solid-body rotation, a result which is expected if the inner morphology is in a quasi-stationary state. Linear least-squares solutions give observed angular velocities of 0.39 ± 0.08 km s^{-1} arcsec^{-1} from spectrum 4M-596 and 0.39 ± 0.05 from spectrum 4M-807. Due to the observed orientation of the galaxy, the observed central angular velocity is less than the true angular velocity. To correct for the effect of projection, we have (Rubin and Ford 1970, eq. [1])

$$\frac{dV(R)}{dR} = \frac{\sec\theta}{\sin i}\frac{dV(s)}{ds} ,$$

where R is the radial coordinate in the plane of the

[1] Operated by Associated Universities, Inc., under contract with the National Science Foundation.

1976ApJ...208..662P

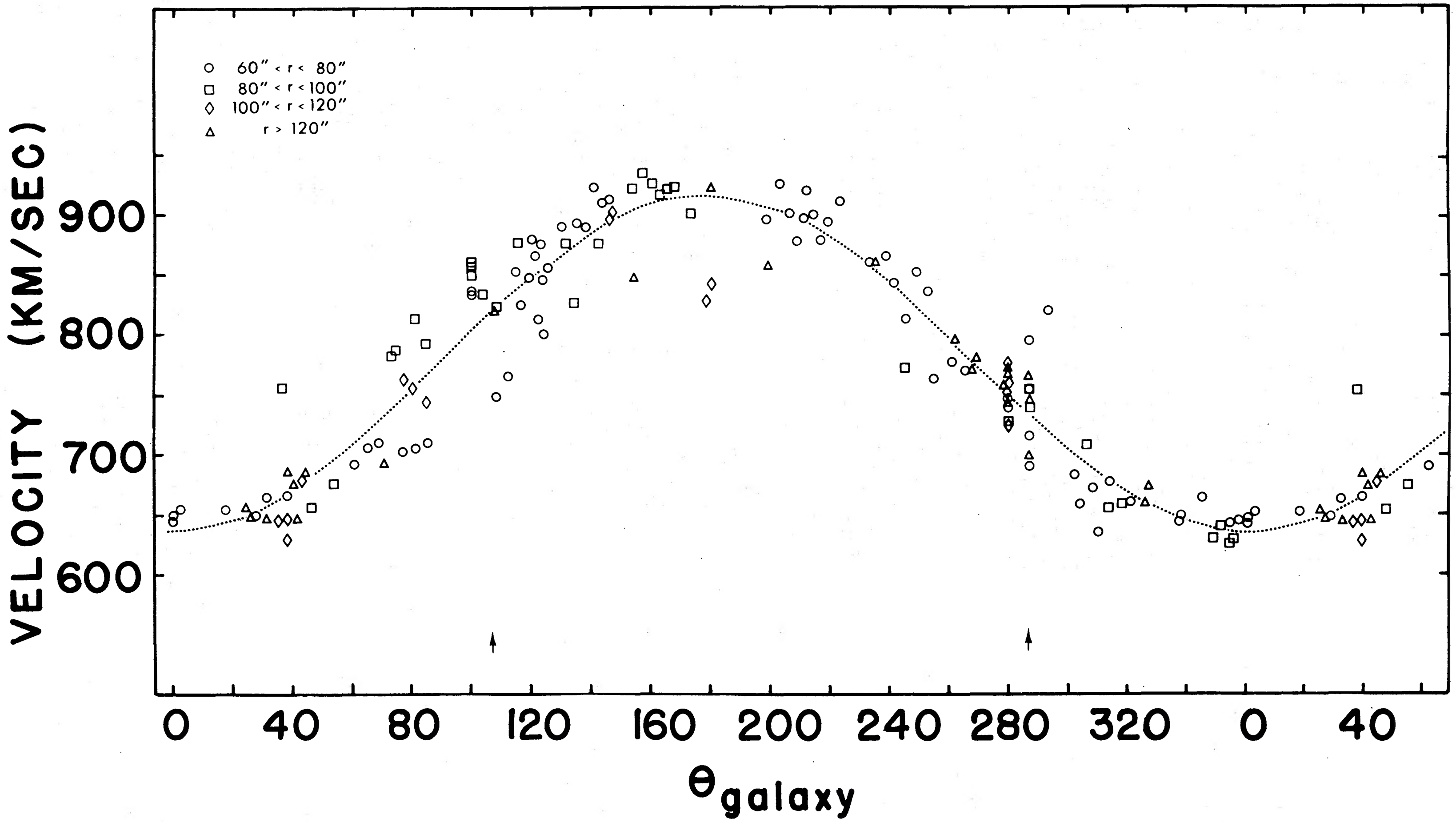

FIG. 4.—Observed line-of-sight hydrogen emission line velocities as a function of angular position (measured from the northeast major axis at P.A. 15° on the sky) in the plane of the galaxy. The dashed line is a least-squares solution with systemic velocity (heliocentric) of 779 ± 3 km s^{-1} and amplitude $V \sin i = 139 \pm 4$ km s^{-1}. Note that the data for $0° < \theta_{\rm galaxy} < 60°$ are repeated. The arrows indicate the position of the bar.

TABLE 4

LEAST-SQUARES SOLUTIONS FOR OBSERVED VELOCITY AS A FUNCTION OF ANGULAR POSITION

Major axis P. A. (degrees)	Radial range (arc sec)	Angular range (degrees)	Mean velocity (km/sec)	Velocity amplitude (km/sec)	Circular velocity (km/sec)	θ_0	RMS error of fit (km/sec)	Number points
18	r>60	0-360	779±3	139±4	216±6	- 2.7±3.7	29	124
	60<r<90	0-360	780±3	143±5	222±8	- 1.8±5.0	31	81
	r>90	0-360	777±4	131±6	204±9	- 3.8±5.5	26	43
15	r>60	0-360	779±3	139±4	216±6	<--held fixed-->	29	124
		0-180	780±4	139±5	216±8		32	72
		180-360	778±4	139±5	216±8		26	52
	60<r<90	0-360	780±3	143±5	222±8		30	82
		0-180	781±5	141±8	219±12		34	44
		180-360	780±4	145±6	226±9		26	38
	r>90	0-360	776±4	130±6	202±9		26	42
		0-180	778±5	136±8	212±12		28	28
		180-360	776±6	113±10	176±16		22	14

galaxy, and s is the radial coordinate on the plane of the sky at position angle θ measured in the plane of the galaxy. For the two respective spectra, $\theta = 78°$ and 83°, and the corrected angular velocities are 2.9 ± 0.6 km s^{-1} arcsec^{-1} and 5.0 ± 0.6 km s^{-1} arcsec^{-1}, with greater weight going to the latter value. We adopt 4 ± 1 km s^{-1} arcsec^{-1} for the central angular velocity, and this value is shown for the inner rotation curve (*heavy line*) in Figure 6. There is a slight indication in Figure 6 of an asymmetry in the rotation curve between the northeast and southwest sides of the galaxy, with the southwest side showing a smaller rotation.

In order to estimate the mass of NGC 3351, a smooth rotation curve was adopted for the galaxy. The distributions of mass and angular momentum were computed from the rotation curve using both a simple disk model (Kuzmin 1952; Perek 1962), and a model in which the equidensity surfaces are similar spheroids (Burbidge, Burbidge, and Prendergast 1959). The mass within a radius of 9.5 kpc is $\sim 6 \times 10^{10}$ $M_\odot$. The total angular momentum to this radius is 8×10^{13} $M_\odot$ km s^{-1} kpc. Both quantities are well within the range of values for masses and angular momenta determined for normal spiral galaxies (Nordsieck 1973).

NGC 3351 was also observed at the 21 cm neutral hydrogen line with the NRAO 91.4 m and the NRAO 42.7 m radio telescopes in September and December of 1975. The profile shown in Figure 5 represents 40 minutes' integration (10 days of observation) in both polarizations on the galaxy with the 91.4 m telescope. The observed integrated flux density is

$$36.2 \text{ Jy km s}^{-1} \text{ (91.4 m telescope, } 10'.3 \times 11'.3 \text{ beam)},$$

$$55.3 \text{ Jy km s}^{-1} \text{ (42.7 m telescope, } 19'.1 \text{ beam)}.$$

The observed difference in integrated flux density is due to the partial resolution of the galaxy by the telescope beam. The ratio of the observed values can be used to estimate the approximate neutral-hydrogen diameter of NGC 3351. Using 40° for the inclination obtained earlier, the half-power neutral-hydrogen diameter along the major axis is 12′, whereas the maximum optical extent measureable on the *National Geographic Society—Palomar Observatory Sky Survey* prints is approximately 8′. Applying a correction factor of 1.3 to the 42.7 m observations because of the angular size of NGC 3351, the corrected integrated flux density is 72 ± 14 Jy km s^{-1}. Using the relation

$$M_{\rm H\,I}/M_\odot = 2.36 \times 10^{19} \times D^2 \int S_V dV\,,$$

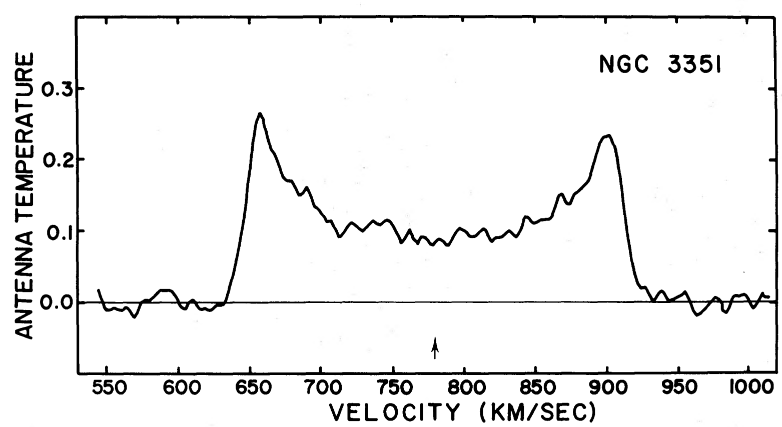

FIG. 5.—The neutral hydrogen velocity profile for NGC 3351, from observations with the NRAO 91 m telescope. The arrow indicates the centroid of the profile at 779 ± 3 km s^{-1}.

1976ApJ...208..662P

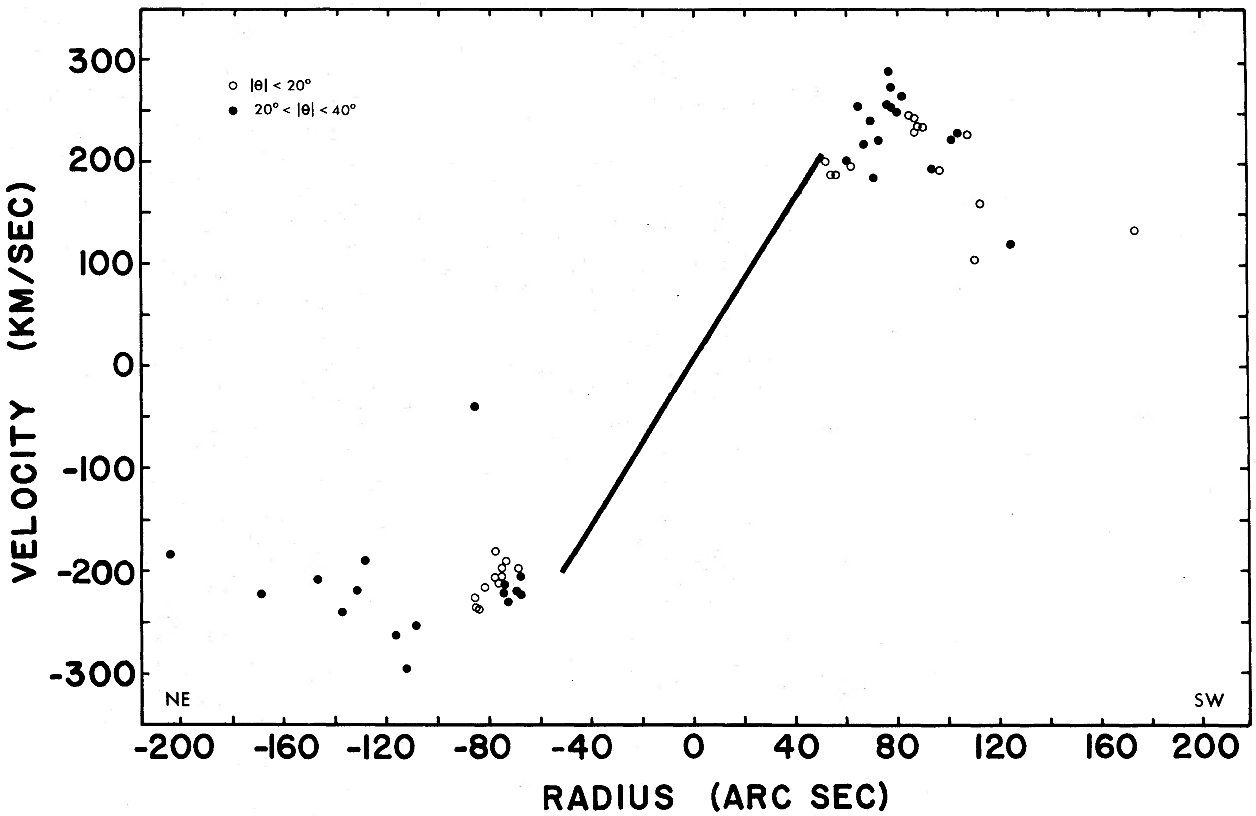

FIG. 6.—The rotation curve of NGC 3351. The solid and open circles represent emission line velocities measured within 40° of the major axis and corrected for the effects of an inclination of 40° to the line of sight. The solid line is the central angular velocity (4 ± 1 km s^{-1} $arcsec^{-1}$) determined from absorption line measurements along the bar.

where D is the distance in parsecs and the integrated flux density is in watts m^{-2} Hz^{-1} km s^{-1} (Roberts 1962), the neutral hydrogen mass of NGC 3351 is 1.7×10^9 $M_\odot$. The ratio of neutral hydrogen to total mass is 0.028, which when compared to 0.053 ± 0.018 obtained from the average of 9 Sb and SBb spiral galaxies (Roberts 1969), indicates that we have not overcorrected our results.

The absorption lines along the bar appear to be narrower than the same features in the nuclear region of M31. If we use 180 km s^{-1} for the velocity dispersion of M31 (Wilson 1975; Faber and Jackson 1976), then the profile of the Mg I feature gives a velocity dispersion of $\sim 140 \pm 30$ (estimated error) km s^{-1}.

IV. DISCUSSION

A comparison of the rotation of NGC 3351 with that of other barred spirals is difficult for a number of reasons. Spectroscopic studies for velocities *from emission lines only* have been made for eight other barred spirals of classical type, but only for four of these objects is there any significant amount of data for the rotation curves over the angular extent of the bars. For NGC 7479 (Burbidge, Burbidge, and Prendergast 1960*a*) and for NGC 925 (Rubin, Burbidge, and Burbidge 1964), spectra along the bars show that the excited gas in this region of the two galaxies is in solid-body rotation. The rotation along the position angle of the bar in NGC 6764 (Rubin, Thonnard, and Ford 1975) is poorly defined, but not inconsistent with a constant angular velocity. That part of the rotation curve of NGC 3504 (Burbidge, Burbidge, and Prendergast 1960*b*) which shows solid-body rotation extends only to the edge of the nucleus. Although the galaxy was classified SBb by Humason, Mayall, and Sandage (1960), the bar is not a well-defined structure, and we would concur with Burbidge, Burbidge, and Prendergast that this object should properly be considered a type intermediate between normal and barred spirals. Spectra of NGC 613 (Burbidge *et al.* 1964) and NGC 5383 (Burbidge, Burbidge, and Prendergast 1962) reveal rapid motions in the nuclei, but emission attributable to excited gas in the bars was not detected. In these two objects, as in the case of NGC 3351, the activity of the excited nuclear gas is not indicative of the kinematics of the stars which comprise the dominant fraction of the mass in the bar. The kinematical evidence at this time suggests that the bars in these galaxies are permanent phenomena, although whether they are stable configurations of matter or are density-waves passing through the constituent matter is a question which is not answered by our observations.

Finally, it must be emphasized that NGC 3351 does not have the difficulty in interpretation of the orientation that is found (Burbidge, Burbidge, and Prendergast 1960*b*, 1962; Burbidge *et al.* 1964; Rubin, Thonnard, and Ford 1975) for barred spiral galaxies whose shape resembles an integral sign. For these forms one cannot assume circular symmetry in order to determine the line of nodes and angle of inclination from the shape of the apparent ellipse formed by the projection of the galaxy on the plane of the sky. It is not even certain that the two arms are coplanar. In NGC 3351, the positions of the kinematical and geometrical major axes coincide, which strongly argues that our assumption of circular symmetry is correct.

V. CONCLUSION

The measurements and analysis of the outer velocity field of NGC 3351 and the results of Paper I lead to the following conclusions:

1. The nuclear region contains a ring of H II regions $r \approx 340$ pc, which is rotating with $V_{\rm rot} = 126 \pm 16$ km s^{-1} and contracting to the nucleus with $V_c = 34 \pm 11$ km s^{-1} (Paper I).

2. The stars in the bar ($r \leq 3$ kpc) are rotating with constant angular velocity 80 ± 20 km s^{-1} kpc^{-1}. The bar is thus a quasi-stationary feature in this galaxy. There is no evidence for excited gas in the bar.

3. Beyond the region of the bar, the velocities of the H II regions within the outer ring reach a maximum of $V_{\rm rot} \approx 220$ km s^{-1} at $R \approx$ 3–5 kpc and then begin to decrease. There is a weak suggestion of rotational asymmetry between the northeast and southwest major axes.

4. A simple mass model for the galaxy gives a total mass and angular momentum consistent with values found for normal spiral galaxies.

We thank Dr. L. Goldberg of KPNO and Dr. D. Heeschen of NRAO for telescope time.

APPENDIX

In discussing velocities determined with any optical system, it is necessary to investigate the systematic errors of that system. Our measuring procedures are identical to those we have employed in the past. A two-dimensional Mann measuring machine with punched card output is used. Each spectrum is accompanied by a "slit curvature plate," taken by putting the comparison spectrum across both the comparison and stellar windows. Systematic curvature effects introduced by the image-tube-plus-camera optical system are corrected for by means of the measures from the slit curvature plate.

From the measures of our 4 m spectra of NGC 3351, we believe the systematic errors to be small:

1. The central velocity $V_c = 779 \pm 3$ km s^{-1} determined from the sinusoidal variation of velocities from 13 spectra taken with the slit tangential to the outer ring agrees with the central velocity $V_c = 779 \pm 8$ km s^{-1} (Rubin, Ford, and Peterson 1975) determined earlier from nuclear spectra taken with the Kitt Peak 84 inch (2.1 m) and Lowell 72 inch (1.8 m) telescopes.

2. The central velocity $V_c = 779 \pm 3$ km s^{-1} determined with the 300 foot NRAO telescope agrees with the optical determinations. Random velocity errors are also assumed to be small, because of the small scatter about the mean sinusoid discussed in (1) above, and shown in Figure 4.

At the telescope the light from the comparison lamp does not have the same optical path as the light from the galaxy and night sky. Hence a more stringent test of the velocity system is to measure night-sky lines in the wavelength interval of interest. We show in Figure 7 (Plate 10) an enlargement of a 4 m spectrum, showing the night-sky features near Hα. On the print we have identified 14 lines; laboratory wavelengths of these lines are given in Table A1. With the exception of Hα in the night sky, the remaining features are all OH lines from the (6, 1)-band system. Wavelengths of individual lines have been taken from Bass and Garvin (1962), and are accurate to better than 0.1 Å. Numerous other compilations of wavelengths of these lines (for example, Blackwell, Ingham, and Rundle 1960; Krassovsky, Shefov, and Yarom 1962; and others) exist, but are of lower accuracy. Measures of several OH lines close to 6550 Å give wavelengths corresponding to velocities in the range +10 to −20 km s^{-1}.

We have insufficient plate material to examine those measures in any detail to see, for example, if the magnitude of this small discrepancy is dependent on grating tilt, or on radial position relative to the camera and intensifier axis, or on the centering of the comparison-source field lens. Because these preliminary results are incomplete, we do not apply an instrumental zero-point correction, but only the slit-curvature correction. Continued attention to the measurement of night-sky features will be necessary to establish the velocity system of this equipment.

TABLE A1

IDENTIFICATION OF NIGHT-SKY LINES NEAR 6550 Å

Line	$\lambda_{\rm air}$	Identification	Intensity*
1..........	6499.06	OH (6, 1) $Q(1)$	S
2..........	6504.81	$Q(2)$	M
3..........	6513.67	$Q(3)$	W
4..........	6522.04	$P_2(2)$	M
5..........	6532.78	$P_1(2)$	S
6..........	6544.20	$P_2(3)$	M
7..........	6553.38	$P_1(3)$	S
8..........	6562.82	Hα	M
9..........	6568.71	OH (6, 1) $P_2(4)$	M
10..........	6577.01	$P_1(4)$	S
11..........	6596.53	$P_2(5)$	W
12..........	6603.76	$P_1(5)$	M
13..........	6627.71	$P_2(6)$	W
14..........	6634.31	$P_1(6)$	M

* S = strong, M = moderate, W = weak.

REFERENCES

Bass, A. M., and Garvin, D. 1962, *J. Molec. Spectrosc.*, **9**, 114.
Blackwell, D. E., Ingham, M. F., and Rundle, H. N. 1960, *Ap. J.*, **131**, 15.
Burbidge, E. M., Burbidge, G. R., and Prendergast, K. H. 1959, *Ap. J.*, **130**, 739.
———. 1960*a*, *ibid.*, **132**, 654.
———. 1960*b*, *ibid.*, p. 661.
———. 1962, *ibid.*, **136**, 704.
Burbidge, E. M., Burbidge, G. R., Rubin, V. C., and Prendergast, K. H. 1964, *Ap. J.*, **140**, 85.
Faber, S. M., and Jackson, R. E. 1976, *Ap. J.*, **204**, 668.
Humason, M. L., Mayall, N. U., and Sandage, A. R. 1960, *A.J.*, **61**, 97.
Krassovsky, V. I., Shefov, N. N., and Yarom, I. 1962, *Planet. and Space Sci.*, **9**, 883.
Kuzmin, G. G. 1952, *Pub. Astr. Obs. Tartu*, **32**, 211.
Moore, C. E. 1959, *A Multiplet Table of Astrophysical Interest*, *NBS Tech. Note* 36.
Nordsieck, K. H. 1973, *Ap. J.*, **184**, 735.
Perek, L. 1962, *Adv. in Astr. and Ap.*, **1**, 165.
Roberts, M. S. 1962, *A.J.*, **67**, 437.
———. 1969, *ibid.*, **74**, 859.
Rubin, V. C., Burbidge, E. M., and Burbidge, G. R. 1964, *Ap. J.*, **140**, 94.
Rubin, V. C., and Ford, W. K., Jr. 1970, *Ap. J.*, **159**, 379.
Rubin, V. C., Ford, W. K., Jr., and Peterson, C. J. 1975, *Ap. J.*, **199**, 39 (Paper I).
Rubin, V. C., Thonnard, N., and Ford, W. K., Jr. 1975, *Ap. J.*, **199**, 31.
Seitter, W. C. 1970, *Atlas für Objektiv Prismen Spektren* (Bonn: Ferd. Dümmlers Verlag).
Vorontsov-Vel'yaminov, B. A., and Savel'eva, M. V. 1974, *Soviet Astr.—AJ*, **17**, 643.
Wilson, C. P. 1975, private communication.

W. Kent Ford, Jr., Charles J. Peterson, Vera C. Rubin, and Norbert Thonnard: Department of Terrestrial Magnetism, Carnegie Institution of Washington, 5241 Broad Branch Road, NW, Washington, DC 20015

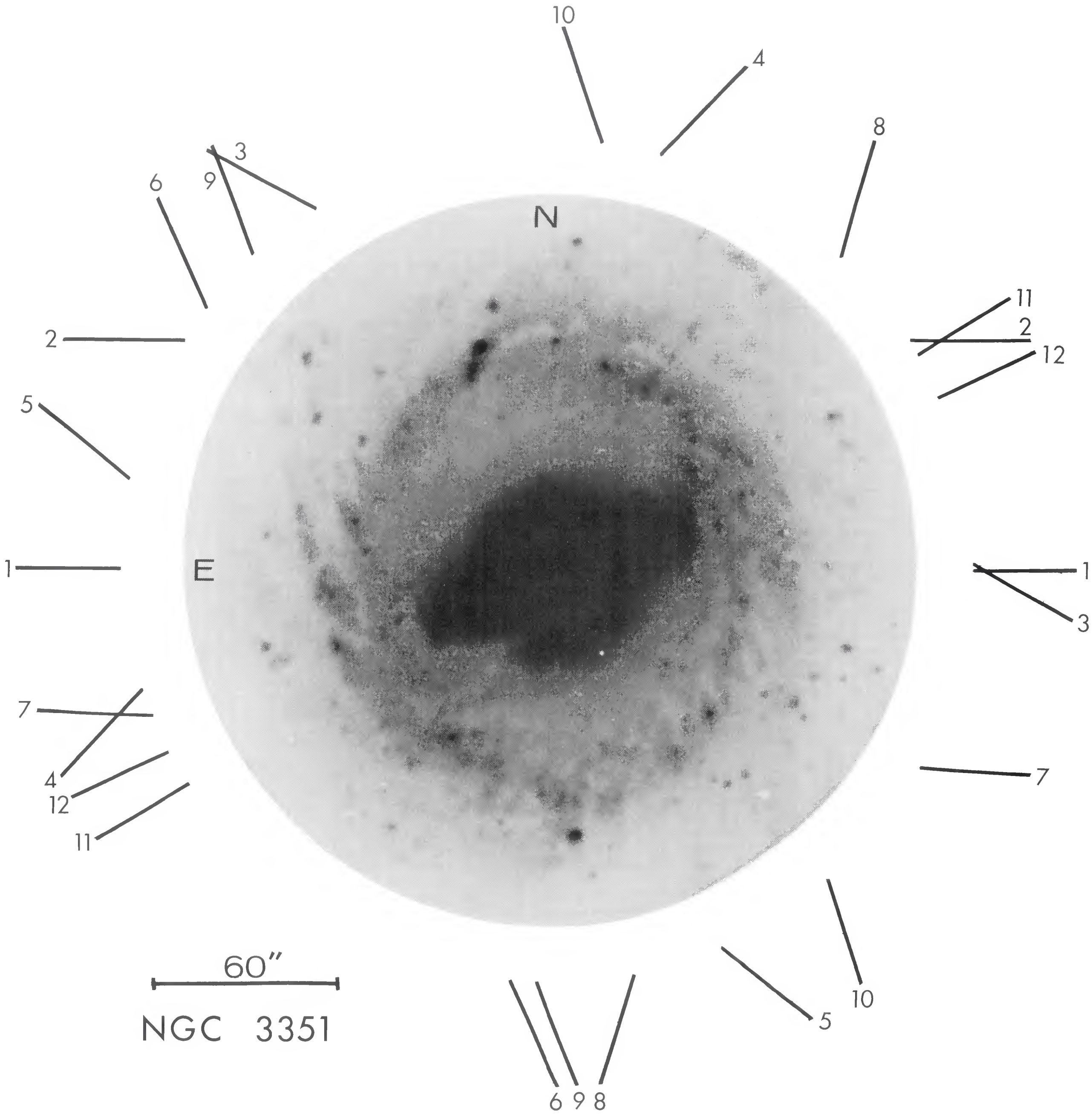

FIG. 1.—NGC 3351, showing the positions of the spectrograph slit for the spectra listed in Table 1. The photograph (4M-RC No. 108) is a 30 s Cassegrain exposure at the 4 m Mayall telescope using a Carnegie image tube and 5030 filter (effective wavelength in the blue).

PETERSON *et al.* (*see* page 664)

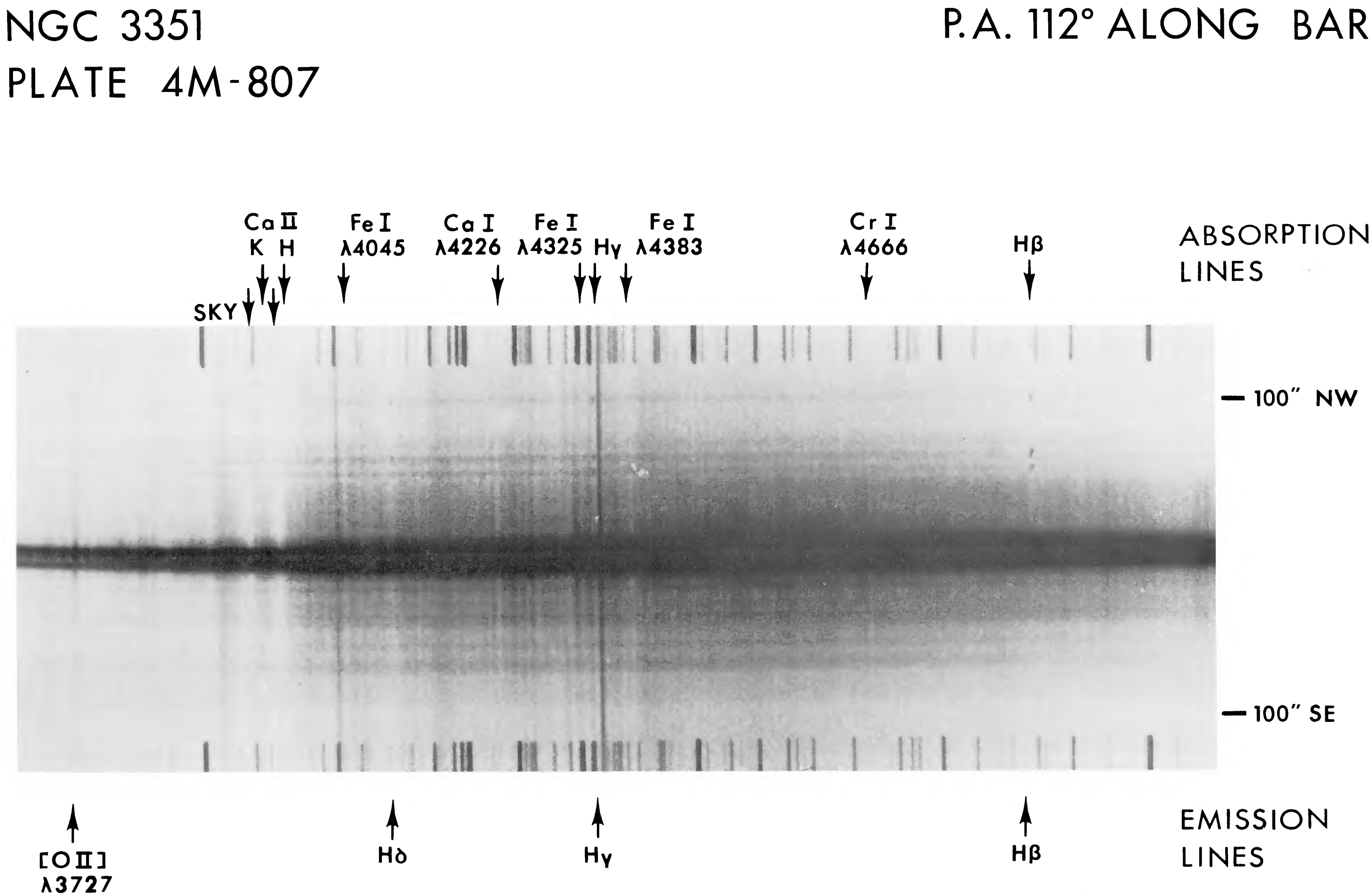

FIG. 2.—The spectrum of NGC 3351 along the bar (position angle 112°). Plate 4M-807, 4 m Mayall telescope + Carnegie image tube, exposure 168 min, original dispersion 40 Å mm⁻¹. The absorption features and emission features measured for velocities are labeled. The displacement of the night-sky absorption lines from the galaxy lines is notable at H, λλ4226, 4383, and 4666.

PETERSON *et al.* (*see* page 664)

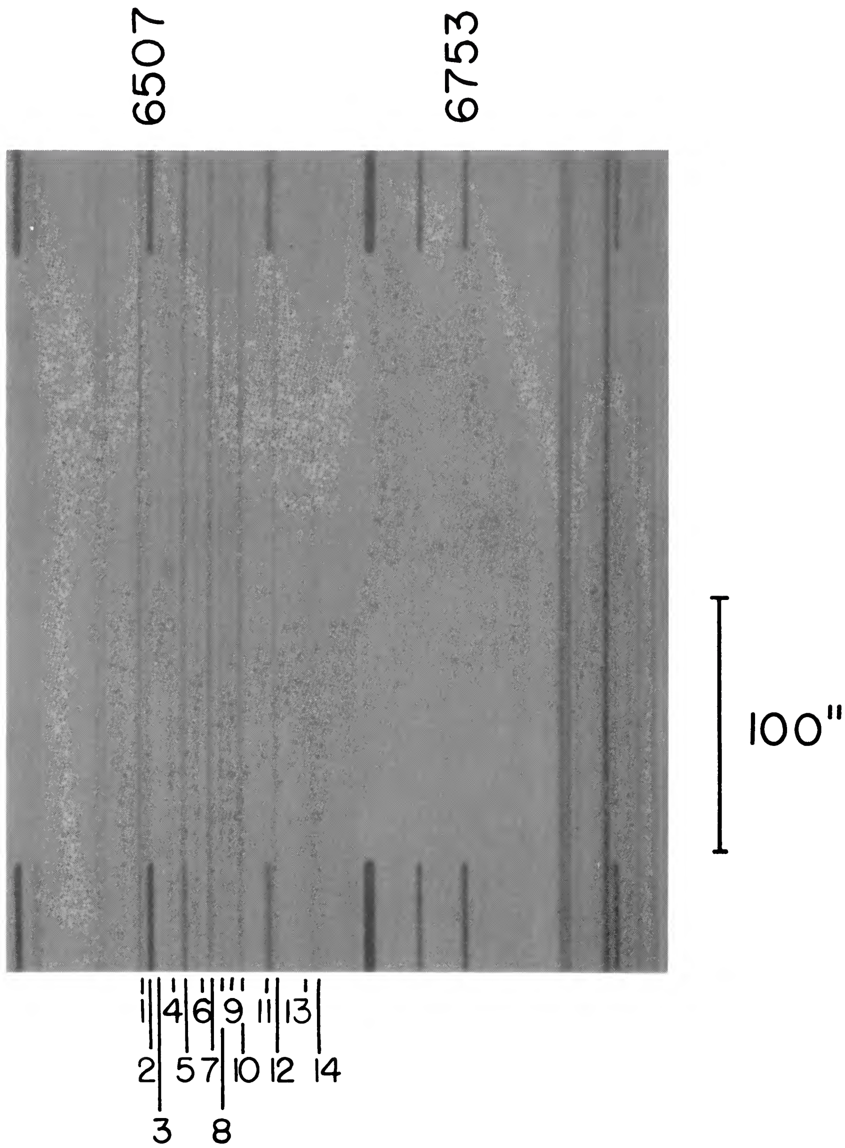

FIG. 7.—Identification of the night-sky spectral lines due to Hα and the (6, 1)-band system of OH. Plate 4M-813, 4 m Mayall telescope + Carnegie image tube, exposure 96 min, original dispersion 52 Å mm^{-1}. The wavelengths of the spectral features are given in Table A1.

PETERSON *et al.* (*see* page 671)